Performance Enhancement in Double-Pendulum Overhead Crane Control: A Fixed-Time Extended State Observer-Based Approach

Hue Luu Thi
Faculty of Electrical Engineering, Electric Power University, Vietnam
huelt@epu.edu.vn (corresponding author)

Received: 14 September | Revised: 14 October 2025, 20 October 2025, and 21 October 2025 | Accepted: 22 October 2025

 DOI: https://doi.org/10.48084/etasr.14777

ABSTRACT

This study presents an effective control solution for a two-Dimensional Double-pendulum Overhead Crane (2DDOC) system, which combines a fixed-time adaptive hierarchical sliding mode controller with a Fixed-Time Extended State Observer (FxT-ESO). First, the 2DDOC model is introduced. Next, the FxT-ESO is analyzed and designed for the 2DDOC system to estimate several state variables, which are difficult to measure directly with sensors, such as the swing velocities of the hook and payload. Based on the system's dynamic model, the fixed-time adaptive hierarchical sliding mode controller was designed under external disturbance conditions, utilizing the state signals provided by the FxT-ESO. The stability of the closed-loop system was analyzed and proven to be stable in fixed-time through Lyapunov stability theory. Finally, simulation scenarios are presented to demonstrate the performance and effectiveness of the proposed observer and controller.

Keywords-double-pendulum crane; fixed-time adaptive hierarchical sliding mode controller; fixed-time extended state observer

I. INTRODUCTION

When compared with fully actuated systems, underactuated systems possess the advantages of reduced cost and enhanced flexibility. Nevertheless, their underactuated and nonlinear nature makes them difficult to control. Most studies on overhead cranes neglect the effect of the hook and consider the payload as a point mass, in which case the payload is assumed to oscillate only according to the motion of the cable [1, 2]. However, the payload still oscillates around the hook when its mass is considerable or when the hook mass cannot be neglected. In such situations, the payload motion can be modeled as a double pendulum [3], which further increases system dynamics complexity. The hoisting/lowering operations of a double pendulum crane can cause significant oscillations, leading to positioning errors and reduced transport efficiency. Research on double-pendulum crane systems has focused on open-loop input–output shaping methods [4, 5], which generate reference trajectories to suppress oscillations. However, the performance of open-loop control may deteriorate under adverse factors in complex working environments. To enhance control robustness, several closed-loop control approaches have been developed for double-pendulum crane systems, such as the reference model-shaping based controller [6], where the trolley position is accurately achieved with small hook and payload oscillations. The auxiliary control input is constructed based on the system dynamics, from which a nonlinear anti-swing control method is designed [7]. The hierarchical sliding mode controller presented in [8, 9] effectively suppresses the swing angles of both the hook and payload. The double-pendulum crane system also faces challenges with system parameters that are difficult to determine accurately and varying payloads. In [10], an adaptive fuzzy PID controller was proposed, which achieved improved control performance. Similarly, authors in [11] introduced an enhanced hierarchical adaptive controller, where multiple oscillation-related states of the pendulum were incorporated into the control input design, thereby improving the sway suppression performance. Authors in [12] designed a sliding surface containing all system states to suppress oscillations and then employed a time-delay estimation to calculate the model parameters. In addition, the system is significantly affected by external disturbances during operation. To address this issue, disturbance observers have been employed to accurately estimate the disturbances [13-15]. Furthermore, not all state variables of the system can be directly measured by sensors, such as the swing velocities of the hook and payload. In [16], a linear state estimator was presented to replace the sensors for measuring swing velocities.

The present study solves both problems. The main contributions of this work are: 1) A novel fixed-time adaptive robust hierarchical sliding mode control method is proposed. This controller is integrated with an FxT-ESO, which effectively estimates lumped disturbances and significantly reduces the number of required sensors. 2) The proposed approach guarantees system stability within a fixed time, providing a clear and predictable upper bound for the settling time, independent of the initial conditions.

II. MODEL OF THE DOUBLE-PENDULUM OVERHEAD CRANE SYSTEM

Figure 1 illustrates the motion of a 2DDOC with the coordinate origin at *OXY*. The crane model consists of a trolley that moves along the *x*-axis, lifting/lowering the payload via a cable. In this study, the cable is assumed to be inextensible. The cable length l_1 varies, whereas l_2 represents the distance from the hook center to the payload center. b_x and b_l are the friction coefficients associated with the trolley motion along the *x*-axis and hoisting mechanism of the cable, respectively. The mathematical description of the 2DDOC system, which uses the Euler-Lagrange formulation, is according to [12]:

$$\boldsymbol{M(q)\ddot{q} + C(q,\dot{q})\dot{q} + G(q) + D = F} \quad (1)$$

where $\boldsymbol{q} = [x,\ l_1,\ \theta_1,\ \theta_2]^T$ is the state vector of the system, $\boldsymbol{M(q)} \in R^{4,4}$ is the inertia matrix, $\boldsymbol{C(q,\dot{q})} \in R^{4,4}$ is the centrifugal and damping matrix, $\boldsymbol{G(q)} \in R^{4,1}$ represents the gravity vector, $\boldsymbol{D} \in R^{4,1}$is the external disturbance vector, and $\mathbf{F} = [F_x\ F_l\ 0\ 0]^T$ represents the control input of the system. The matrices and vectors of the system are described in [12].

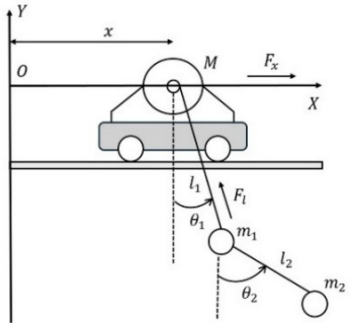

Fig. 1. Dynamic model of the 2DDOC system.

III. FIXED-TIME EXTENDED STATE OBSERVER FOR 2DDOC

In the crane system, some state variables, such as the velocity of the hook and the swing velocity of the payload, are difficult to measure. Additionally, the system is affected by external disturbances. This section addresses these issues by designing an FxT-ESO to estimate both the state variables and the lumped disturbance.

The dynamic equation (1) of the 2DDOC system can be expressed as:

$$\ddot{\boldsymbol{q}} = \boldsymbol{M^{-1}(q)F - M^{-1}(q)\big(C(q,\dot{q})\dot{q} + G(q)\big)} \\ \boldsymbol{-M^{-1}(q)D} \quad (2)$$

The state vector of the system is defined as $\boldsymbol{z} = [\boldsymbol{z}_1\boldsymbol{z}_2]^T = [\boldsymbol{q}\dot{\boldsymbol{q}}]^T$, and the dynamic system (2) is represented in the state-space form as:

$$\begin{cases} \dot{\boldsymbol{z}}_1 &= \boldsymbol{z}_2 \\ \dot{\boldsymbol{z}}_2 &= \boldsymbol{z}_3 + \boldsymbol{M^{-1}(q)F} \\ \dot{\boldsymbol{z}}_3 &= \Omega(t) \end{cases} \quad (3)$$

where $\Omega(t)$ is the time derivative of the lumped disturbance and

$$\boldsymbol{z}_3 = \boldsymbol{d}(t) = \boldsymbol{-M^{-1}(q)(C(q,\dot{q})\dot{q} + G(q)) - M^{-1}(q)D}$$

Assumption 1: The lumped disturbance and its time derivative are continuous and bounded. Therefore, positive constants $\varepsilon_1, \varepsilon_2$ exist satisfying:$\|\boldsymbol{d}(t)\| \le \varepsilon_1$ and $\|\dot{\boldsymbol{d}}(t)\| \le \varepsilon_2$.

The FxT-ESO is designed for the system as:

$$\begin{cases} \dot{\hat{\boldsymbol{z}}}_1 = \hat{\boldsymbol{z}}_2 + \boldsymbol{\kappa}_1\mathrm{sig}^{\gamma_1}\tilde{\boldsymbol{z}}_1 + \boldsymbol{\kappa}_1\mathrm{sig}^{\gamma_2}\tilde{\boldsymbol{z}}_1 \\ \dot{\hat{\boldsymbol{z}}}_2 = \hat{\boldsymbol{z}}_3 + \boldsymbol{\kappa}_2\mathrm{sig}^{2\gamma_1-1}\tilde{\boldsymbol{z}}_1 + \\ \qquad \boldsymbol{\kappa}_2\mathrm{sig}^{2\gamma_2-1}\tilde{\boldsymbol{z}}_1 + \boldsymbol{M^{-1}(z_1)F} \\ \dot{\hat{\boldsymbol{z}}}_3 = \boldsymbol{\kappa}_3\mathrm{sig}^{3\gamma_1-2}\tilde{\boldsymbol{z}}_1 + \\ \qquad \boldsymbol{\kappa}_3\mathrm{sig}^{3\gamma_2-2}\tilde{\boldsymbol{z}}_1 + \Lambda\mathrm{sign}(\tilde{\boldsymbol{z}}_1) \end{cases} \quad (4)$$

where $\hat{\boldsymbol{z}}_i$ is the estimate of $\boldsymbol{z}_i$, $\boldsymbol{\kappa}_i$ is the diagonal coefficient matrix, the estimation error is $\tilde{\boldsymbol{z}}_i = \boldsymbol{z}_i - \hat{\boldsymbol{z}}_i$, $(i = 1 \div 3)$, Λ is the observer gain satisfying: $\Lambda > \varepsilon_2$, $\gamma_1 \in (1-\varrho_1, 1)$, $\gamma_2 \in (1, 1+\varrho_2)$, with ϱ_1 and ϱ_2 being sufficiently small positive values. The gain matrices are chosen such that the matrix $\boldsymbol{A}$ is Hurwitz:

$$\boldsymbol{A} = \begin{bmatrix} -\boldsymbol{\kappa}_1 & \boldsymbol{I}_{4\times4} & \boldsymbol{0}_{4\times4} \\ -\boldsymbol{\kappa}_2 & \boldsymbol{0}_{4\times4} & \boldsymbol{I}_{4\times4} \\ -\boldsymbol{\kappa}_3 & \boldsymbol{0}_{4\times4} & \boldsymbol{0}_{4\times4} \end{bmatrix}$$

The symmetric positive definite matrices $\boldsymbol{P}$ and $\boldsymbol{Q}$ satisfy:

$$\boldsymbol{A^TP + PA = -Q}$$

From (3) and (4), the observation error is defined as:

$$\begin{cases} \dot{\tilde{\boldsymbol{z}}}_1 = \tilde{\boldsymbol{z}}_2 - \boldsymbol{\kappa}_1\mathrm{sig}^{\gamma_1}\tilde{\boldsymbol{z}}_1 - \boldsymbol{\kappa}_1\mathrm{sig}^{\gamma_2}\tilde{\boldsymbol{z}}_1 \\ \dot{\tilde{\boldsymbol{z}}}_2 = \tilde{\boldsymbol{z}}_3 - \boldsymbol{\kappa}_2\mathrm{sig}^{2\gamma_1-1}\tilde{\boldsymbol{z}}_1 - \boldsymbol{\kappa}_2\mathrm{sig}^{2\gamma_2-1}\tilde{\boldsymbol{z}}_1 + \\ \dot{\tilde{\boldsymbol{z}}}_3 = -\boldsymbol{\kappa}_3\mathrm{sig}^{3\gamma_1-2}\tilde{\boldsymbol{z}}_1 - \\ \qquad \boldsymbol{\kappa}_3\mathrm{sig}^{3\gamma_2-2}\tilde{\boldsymbol{z}}_1 - \Lambda\mathrm{sign}(\tilde{\boldsymbol{z}}_1) + \Omega(t) \end{cases} \quad (5)$$

Theorem 3.1: *The FxT-ESO (4) is applied to the 2DDOC system (1). The FxT-ESO guarantees that the observation errors $\tilde{\boldsymbol{z}}_1$ and $\tilde{\boldsymbol{z}}_2$ converge to zero within the fixed time T_f, and at the same time, the estimation error of the lumped disturbance $\tilde{\boldsymbol{z}}_3$ also converges to a neighborhood of zero within the same time T_f.*

Proof: The observation error, as described in (5), can be decomposed into two components. In the initial stage, the significant difference between the actual and the estimated values, with the primary contribution from the coefficient γ_2, drives the rapid decay of the error. Therefore, the analysis begins with this subsystem:

$$\begin{cases} \dot{\tilde{\boldsymbol{z}}}_1 = \tilde{\boldsymbol{z}}_2 - \boldsymbol{\kappa}_1\mathrm{sig}^{\gamma_2}\tilde{\boldsymbol{z}}_1 \\ \dot{\tilde{\boldsymbol{z}}}_2 = \tilde{\boldsymbol{z}}_3 - \boldsymbol{\kappa}_2\mathrm{sig}^{2\gamma_2-1}\tilde{\boldsymbol{z}}_1 \\ \dot{\tilde{\boldsymbol{z}}}_3 = -\boldsymbol{\kappa}_3\mathrm{sig}^{3\gamma_2-2}\tilde{\boldsymbol{z}}_1 \end{cases} \quad (6)$$

The Lyapunov candidate function is chosen as:

$$V_{\gamma_2}(\gamma_2, \tilde{\boldsymbol{z}}) = \boldsymbol{\zeta}_{\gamma_2}^T\boldsymbol{P}\boldsymbol{\zeta}_{\gamma_2} \quad (7)$$

With:

$$\tilde{\boldsymbol{z}} = [\tilde{\boldsymbol{z}}_1^T, \tilde{\boldsymbol{z}}_2^T, \tilde{\boldsymbol{z}}_3^T]^T$$

$$\boldsymbol{\zeta}_{\gamma_2} = \left[(\tilde{\boldsymbol{z}}_1^{1/\gamma_2})^T, (\tilde{\boldsymbol{z}}_2^{1/(2\gamma_2-1)})^T, (\tilde{\boldsymbol{z}}_3^{1/(3\gamma_2-2)})^T\right]^T$$

If γ_2 is chosen as 1, then the observation error of the system is given by: $\dot{\boldsymbol{\zeta}}_{\gamma_2} = \boldsymbol{A}\boldsymbol{\zeta}_{\gamma_2}$. Therefore, the time derivative of $V_{\gamma_2}(\gamma_2, \tilde{\boldsymbol{z}})$ is obtained by:

$$\dot{V}_{\gamma_2}(1, \tilde{\boldsymbol{z}}) = \dot{\boldsymbol{\zeta}}_{\gamma_2}^T \boldsymbol{P}\boldsymbol{\zeta}_{\gamma_2} + \boldsymbol{\zeta}_{\gamma_2}^T \boldsymbol{P}\dot{\boldsymbol{\zeta}}_{\gamma_2} = -\boldsymbol{\zeta}_{\gamma_2}^T \boldsymbol{Q}\boldsymbol{\zeta}_{\gamma_2} \leqslant \boldsymbol{\zeta}_{\gamma_2}^T \lambda_{\min}(\boldsymbol{Q})\boldsymbol{\zeta}_{\gamma_2} \leqslant 0 \quad (8)$$

where $\lambda_{\min}(\boldsymbol{Q})$ denotes the minimum eigenvalue of $\boldsymbol{Q}$. According to [17], the function $V_{\gamma_2}(\gamma_2, \tilde{\boldsymbol{z}})$ serves as a Lyapunov function for (6). If a small positive constant ϱ_2 exists such that $\gamma_2 \in (1, 1 + \varrho_2)$, it can be shown that the observation error in (6) is asymptotically stable. Furthermore, according to Lemma 4 in [18], the time derivative of the Lyapunov candidate $V_{\gamma_2}(\gamma_2, \tilde{\boldsymbol{z}})$ is given by:

$$\dot{V}_{\gamma_2}(\gamma_2, \tilde{\boldsymbol{z}}) \leqslant \frac{-\lambda_{min}(\boldsymbol{Q})}{2\lambda_{max}(\boldsymbol{P})} V_{\gamma_2}^{(\gamma_2+1)/2}(\gamma_2, \tilde{\boldsymbol{z}}) \quad (9)$$

Subsequently, as the observation error decreases, the gain γ_1 facilitates the convergence of the observation errors to zero. The latter part of equation (5) is given by:

$$\begin{cases} \dot{\tilde{\boldsymbol{z}}}_1 = \tilde{\boldsymbol{z}}_2 - \boldsymbol{\kappa}_1 \mathrm{sig}^{\gamma_1}\tilde{\boldsymbol{z}}_1 \\ \dot{\tilde{\boldsymbol{z}}}_2 = \tilde{\boldsymbol{z}}_3 - \boldsymbol{\kappa}_2 \mathrm{sig}^{2\gamma_1 - 1}\tilde{\boldsymbol{z}}_1 \\ \dot{\tilde{\boldsymbol{z}}}_3 = -\boldsymbol{\kappa}_3 \mathrm{sig}^{3\gamma_1 - 2}\tilde{\boldsymbol{z}}_1 \end{cases} \quad (10)$$

Similar to the first component, it can be readily shown that the system described by (10) achieves finite-time convergence, and the time derivative of the second Lyapunov candidate $V_{\gamma_1}(\gamma_1, \tilde{\boldsymbol{z}})$ satisfies the following condition:

$$\dot{V}_{\gamma_1}(\gamma_1, \tilde{\boldsymbol{z}}) \leqslant \frac{-\lambda_{min}(\boldsymbol{Q})}{2\lambda_{max}(\boldsymbol{P})} V_{\gamma_1}^{(\gamma_1+1)/2}(\gamma_1, \tilde{\boldsymbol{z}}) \quad (11)$$

Based on Theorem 2 in [17], the estimation error $\tilde{\boldsymbol{z}}_i$ converges to zero or to a neighborhood of zero within the fixed time T_o:

$$T_o \leqslant \frac{\lambda_{\max}(\boldsymbol{P})}{\lambda_{\min}(\boldsymbol{Q})} \left[\frac{\lambda_{\max}^{1-\gamma_1}(\boldsymbol{P})}{1-\gamma_1} + \frac{1}{(\gamma_2 - 1)Y^{\gamma_2 - 1}} \right] \quad (12)$$

where Y is a positive constant that satisfies the condition $Y \leqslant \lambda_{\min}(\boldsymbol{P})$. The convergence of $\tilde{\boldsymbol{z}}_1$ to zero at T_o will continue thereafter, meaning that $\dot{\tilde{\boldsymbol{z}}}_1 = 0$ and $\tilde{\boldsymbol{z}}_2 = \tilde{\boldsymbol{z}}_3 = 0$. Therefore, there is a time instant T_o, such that $\tilde{\boldsymbol{z}}_1 = \tilde{\boldsymbol{z}}_2 = \tilde{\boldsymbol{z}}_3 = 0$ for all $t \geqslant T_o$. According to [19], the following equation can be obtained:

$$\dot{\tilde{\boldsymbol{z}}}_3 = -\Lambda \mathrm{sign}(\tilde{\boldsymbol{z}}_1) + \Omega(t) = 0 \forall t \geq T_o \quad (13)$$

Although $\tilde{\boldsymbol{z}}_3$ does not converge exactly to zero due to various factors, such as sampling, delays, and the lumped disturbance $\Omega(t)$, authors in [20] show the existence of a small convergence region $\tilde{\boldsymbol{z}}_3|_R$, which allows $\tilde{\boldsymbol{z}}_3$ to reach the region $\tilde{\boldsymbol{z}}_3|_R$ within the fixed time T_d:

$$T_d = \frac{\tilde{\boldsymbol{z}}_3|_R}{\Lambda - \varepsilon_2} \quad (14)$$

Thus, the upper bound of the convergence time for the FxT-ESO is given by $T_f = T_o + T_d$. With this, the proof of Theorem 3.1 is complete.

IV. FIXED-TIME ADAPTIVE HIERARCHICAL SLIDING MODE CONTROL BASED ON FXT-FSO

The main objective of this study is to design the control input $\boldsymbol{U}_a = [F_x F_l]^T$ such that the state variables reach their reference values $\boldsymbol{q}_r = [x_r l_{1r} \theta_{1r} \theta_{2r}]^T$. Due to the underactuated nature of the 2DDOC system, the system dynamics are divided into two subsystems: one for the actuated states $\boldsymbol{q}_a = [x l_1]^T$, and the other for the underactuated states $\boldsymbol{q}_u = [\theta_1 \theta_2]^T$:

$$\boldsymbol{M}_{a1}(\boldsymbol{q})\ddot{\boldsymbol{q}}_a + \boldsymbol{M}_{u1}(\boldsymbol{q})\ddot{\boldsymbol{q}}_u + \boldsymbol{M}_{a1}(\boldsymbol{q})\boldsymbol{H}_a + \boldsymbol{M}_{u1}(\boldsymbol{q})\boldsymbol{H}_u = \boldsymbol{U}_a \quad (15)$$

$$\boldsymbol{M}_{a2}(\boldsymbol{q})\ddot{\boldsymbol{q}}_a + \boldsymbol{M}_{u2}(\boldsymbol{q})\ddot{\boldsymbol{q}}_u + \boldsymbol{M}_{a2}(\boldsymbol{q})\boldsymbol{H}_a + \boldsymbol{M}_{u2}(\boldsymbol{q})\boldsymbol{H}_u = 0 \quad (16)$$

where $\boldsymbol{M}_{a1}(\boldsymbol{q}) \in R^{2,2}$, $\boldsymbol{M}_{u1}(\boldsymbol{q}) \in R^{2,2}$, $\boldsymbol{M}_{a2}(\boldsymbol{q}) \in R^{2,2}$ and $\boldsymbol{M}_{u2}(\boldsymbol{q}) \in R^{2,2}$ are determined from the matrix $\boldsymbol{M}(\boldsymbol{q})$, $\boldsymbol{H} = [\boldsymbol{H}_a \boldsymbol{H}_u]^T = \boldsymbol{M}^{-1}(\boldsymbol{q})(\boldsymbol{C}(\boldsymbol{q}, \dot{\boldsymbol{q}}) + \boldsymbol{G}(\boldsymbol{q}) + \boldsymbol{D})$.

From (16), by first eliminating the variable $\ddot{\boldsymbol{q}}_u$ in (15) and then $\ddot{\boldsymbol{q}}_a$, the equivalent dynamic model of the system can be derived as:

$$\begin{cases} \boldsymbol{M}_a(\boldsymbol{q})\ddot{\boldsymbol{q}}_a + \boldsymbol{M}_a(\boldsymbol{q})\boldsymbol{H}_a = \boldsymbol{U}_a \\ \boldsymbol{M}_u(\boldsymbol{q})\ddot{\boldsymbol{q}}_u + \boldsymbol{M}_u(\boldsymbol{q})\boldsymbol{H}_u = \boldsymbol{U}_a \end{cases} \quad (17)$$

with $\boldsymbol{M}_a = \boldsymbol{M}_{a1} - \boldsymbol{M}_{u1}\boldsymbol{M}_{u2}^{-1}\boldsymbol{M}_{a2}$ and $\boldsymbol{M}_u = \boldsymbol{M}_{u1} - \boldsymbol{M}_{a1}\boldsymbol{M}_{a2}^{-1}\boldsymbol{M}_{u2}$.

The auxiliary sliding surface takes the estimated state of the 2DDOC as input and is defined as:

$$\begin{cases} s_a = \hat{\boldsymbol{z}}_{2a} - \dot{\boldsymbol{q}}_{ar} + \boldsymbol{K}_{a1}\psi_a(\boldsymbol{e}_a) + \boldsymbol{K}_{a2}\Delta_a(\boldsymbol{e}_a) \\ s_u = \hat{\boldsymbol{z}}_{2u} - \dot{\boldsymbol{q}}_{ur} + \boldsymbol{K}_{u1}\psi_u(\boldsymbol{e}_u) + \boldsymbol{K}_{u2}\Delta_u(\boldsymbol{e}_a) \end{cases} \quad (18)$$

where $\hat{\boldsymbol{z}}_{2a} = [\hat{\boldsymbol{z}}_2(1)\hat{\boldsymbol{z}}_2(2)]^T$, $\hat{\boldsymbol{z}}_{2u} = [\hat{\boldsymbol{z}}_2(3)\hat{\boldsymbol{z}}_2(4)]^T$ is the estimated value of $\dot{\boldsymbol{q}}_a = \boldsymbol{z}_{2a}$, $\dot{\boldsymbol{q}}_u = \boldsymbol{z}_{2u}$, $\boldsymbol{q}_{ar} = [x_r l_{1r}]^T$, $\boldsymbol{q}_{ur} = [00]^T$ represents the reference trajectory, $\boldsymbol{e}_a = \boldsymbol{q}_a - \boldsymbol{q}_{ar} = [e_1 \; e_2]^T$ and $\boldsymbol{e}_u = \boldsymbol{q}_u - \boldsymbol{q}_{ur} = [e_3 e_4]^T$ are tracking errors, $\psi_a(\boldsymbol{e}_a) = [\psi_1 \psi_2]^T$, $\psi_u(\boldsymbol{e}_a) = [\psi_3 \psi_4]^T$, $\Delta_a(\boldsymbol{e}_a) = [\Delta_1 \Delta_2]^T$, $\Delta_u(\boldsymbol{e}_a) = [\Delta_3 \Delta_4]^T$, where:

$\psi_i = \begin{cases} \mathrm{sig}^{\alpha_{1i}}(e_i) |e_i| > \sigma_i \\ \nu_{1i} e_i + \mu_{1i} e_i^2 \mathrm{sgn}(e_i) |e_i| < \sigma_i. \end{cases}$, $\alpha_{1i} = N_1^{\mathrm{sgn}(|e_i|-1)}$, $N_1 > 1$, $\nu_{1i} = (2 - \alpha_{1i})\sigma_i^{\alpha_{1i}-1}$, $\mu_{1i} = (\alpha_{1i} - 1)\sigma_i^{\alpha_{1i}-2}$, $\Delta_i = \begin{cases} \mathrm{sig}^{\alpha_{2i}}(e_i) |e_i| > \sigma_i \\ \nu_{2i} e_i + \mu_{2i} e_i^2 \mathrm{sgn}(e_i) |e_i| < \sigma_i. \end{cases}$, $\alpha_{2i} = N_2^{\mathrm{sgn}(1-|e_i|)}$, $0 < N_2 < 1$, $\nu_{2i} = (2 - \alpha_{2i})\sigma_i^{\alpha_{2i}-1}$, $\mu_{2i} = (\alpha_{2i} - 1)\sigma_i^{\alpha_{2i}-2}$, σ_i denotes a small positive constant ($i = 1 \div 4$), and $\boldsymbol{K}_{a1}$, $\boldsymbol{K}_{a2}$, $\boldsymbol{K}_{u1}$, $\boldsymbol{K}_{u2}$ are positive definite constant matrices.

The proposed sliding surface is defined as:

$$\boldsymbol{s} = \boldsymbol{s}_a + \boldsymbol{\xi}\boldsymbol{s}_u \quad (19)$$

where $\boldsymbol{\xi}$ is a constant matrix.

Based on the information provided by the FxT-ESO, the fixed time hierarchical sliding mode controller is proposed as:

$$\boldsymbol{U}_a = -\left(\boldsymbol{M}_a^{-1}(\boldsymbol{q}) + \boldsymbol{\xi}\boldsymbol{M}_u^{-1}(\boldsymbol{q})\right)^{-1}[\hat{\boldsymbol{z}}_{3a} - \ddot{\boldsymbol{q}}_{ar} + \boldsymbol{K}_{a1}\hat{\tilde{\psi}}_a(\boldsymbol{e}_a) + \boldsymbol{K}_{a2}\hat{\Delta}_a(\boldsymbol{e}_a) + \boldsymbol{\xi}\left(\hat{\boldsymbol{z}}_{3u} - \ddot{\boldsymbol{q}}_{ur} + \boldsymbol{K}_{u1}\hat{\tilde{\psi}}_u(\boldsymbol{e}_u) + \boldsymbol{K}_{u2}\hat{\Delta}_u(\boldsymbol{e}_u)\right) + \boldsymbol{\Gamma}_1\mathrm{sig}^{M_1}(\boldsymbol{s}) + \boldsymbol{\Gamma}_2\mathrm{sig}^{M_2}(\boldsymbol{s}) + \Gamma_3\boldsymbol{s} + \boldsymbol{\Gamma}_4\mathrm{sgn}(\boldsymbol{s})] \quad (21)$$

where $\boldsymbol{\Gamma_i}$ $(i = 1 \div 3)$ is a positive definite control parameter matrix, $\boldsymbol{\Gamma}_4$ is a positive control parameter, $M_1 > 1$, and $0 < M_2 < 1$.

Theorem 4.1: *Consider the 2DDOC system (1) under the observer (4) and the controller (21). Then, the closed-loop system is fixed-time stable with the convergence time* T_{fc}.

Proof: The proposed Lyapunov function is given by:

$$V_c = \frac{1}{2}\boldsymbol{s}^T\boldsymbol{s} \quad (22)$$

Taking the time derivative of (22), then substituting (20) and (21), and after some steps of manipulation, we obtain:

$$\dot{V}_c = \boldsymbol{s}^T\dot{\boldsymbol{s}} = \boldsymbol{s}^T\left(\boldsymbol{K}_{a1}\tilde{\tilde{\psi}}_a(\boldsymbol{e}_a) + \boldsymbol{K}_{a2}\tilde{\tilde{\Delta}}_a(\boldsymbol{e}_a) + \kappa_2\mathrm{sig}^{2\gamma_1-1}(\tilde{\boldsymbol{z}}_{1a}) + \kappa_2\mathrm{sig}^{2\gamma_2-1}(\tilde{\boldsymbol{z}}_{1a}) + \boldsymbol{\xi}\left(\boldsymbol{K}_{u1}\tilde{\tilde{\psi}}_u(\boldsymbol{e}_a) + \boldsymbol{K}_{u2}\tilde{\tilde{\Delta}}_u(\boldsymbol{e}_a) + \kappa_2(\mathrm{sig}^{2\gamma_1-1}(\tilde{\boldsymbol{z}}_{1u}) + \mathrm{sig}^{2\gamma_2-1}(\tilde{\boldsymbol{z}}_{1u})) - \boldsymbol{\Gamma}_1\mathrm{sig}^{M_1}(\boldsymbol{s}) - \boldsymbol{\Gamma}_2\mathrm{sig}^{M_2}(\boldsymbol{s}) - \boldsymbol{\Gamma}_3\boldsymbol{s} - \boldsymbol{\Gamma}_4\mathrm{sgn}(\boldsymbol{s})\right) \quad (23)$$

where $\tilde{\tilde{\psi}}_a = \dot{\psi}_a - \hat{\tilde{\psi}}_a$, $\tilde{\tilde{\psi}}_u = \dot{\psi}_u - \hat{\tilde{\psi}}_u$, $\tilde{\tilde{\Delta}}_a = \dot{\Delta}_a - \hat{\tilde{\Delta}}_a$, $\tilde{\tilde{\Delta}}_u = \dot{\Delta}_u - \hat{\tilde{\Delta}}_u$.

It follows from Theorem 3.1 that after the time T_f, the observation errors converge to zero, which means $\tilde{\boldsymbol{z}}_1 = 0$ and $\tilde{\boldsymbol{z}}_2 = 0$. Hence, (23) can be rewritten as:

$$\dot{V}_c \leqslant -\boldsymbol{s}^T(\boldsymbol{\Gamma}_1\mathrm{sig}^{M_1}(\boldsymbol{s}) + \boldsymbol{\Gamma}_2\mathrm{sig}^{M_2}(\boldsymbol{s}) + \boldsymbol{\Gamma}_3\boldsymbol{s}) \leqslant \boldsymbol{\Gamma}_1^*V_c^{(M_1+1)/2} - \boldsymbol{\Gamma}_2^*V_c^{(M_2+1)/2} - \boldsymbol{\Gamma}_3^*V \quad (24)$$

where $\boldsymbol{\Gamma}_1^* = 2^{(M_1+1)/2}\boldsymbol{\Gamma}_1$, $\boldsymbol{\Gamma}_2^* = 2^{(M_2+1)/2}\boldsymbol{\Gamma}_2$, $\boldsymbol{\Gamma}_3^* = 2\boldsymbol{\Gamma}_3$, with $\boldsymbol{\Gamma}_1$, $\boldsymbol{\Gamma}_2$, and $\boldsymbol{\Gamma}_3$. According to [21], the Lyapunov function given in (22) converges to zero within a fixed time T_c, whose upper bound is determined by:

$$T_c \leq \frac{2}{\boldsymbol{\Gamma}_3^*(M_1-1)}ln\left(1 + \frac{\boldsymbol{\Gamma}_3^*}{\boldsymbol{\Gamma}_1^*}\right) + \frac{2}{\boldsymbol{\Gamma}_3^*(1-M_2)}ln\left(1 + \frac{\boldsymbol{\Gamma}_3^*}{\boldsymbol{\Gamma}_2^*}\right) \quad (25)$$

Theorem 3.1 guarantees that the observation errors converge within a fixed time T_f. The controller converges within a fixed time T_c. Therefore, the overall convergence time of the system is $T_r = T_f + T_c$. For all $t \geq T_r$, the sliding surface $\boldsymbol{s}$ converges to zero. According to [22], $\boldsymbol{s}_a$ and $\boldsymbol{s}_u$ also converge to zero.

Therefore, the closed-loop system is fixed-time stable $T_{fc} = T_r$, which completes the proof of Theorem 4.1.

V. SIMULATION RESULTS

Simulations were performed in MATLAB/Simulink to evaluate the performance of the proposed controller and observer. To demonstrate the adaptability and robustness of controller (21), two simulation scenarios were implemented.

- Scenario 1: The controller's adaptability is evaluated by doubling the system matrices and vectors $\boldsymbol{M}(\boldsymbol{q})$, $\boldsymbol{C}(\boldsymbol{q},\dot{\boldsymbol{q}})$, and $\boldsymbol{G}(\boldsymbol{q})$. Simultaneously, the initial swing angles of the hook and payload were set to non-zero values when the system began to move.
- Scenario 2: The robustness of the controller, as well as the extended state estimation capability of the observer, are demonstrated when the system is subjected to external disturbances.

The parameters for the system, observer, and controller are listed in Table I:

TABLE I. PARAMETERS FOR SCENARIO 2

Parameter	Value
M	5 kg
m_1	1 kg
m_2	5 kg
l_2	0.2 m
b_x	82 Ns/m
b_l	75 Ns/m
g	9.8 m/s^2
$\boldsymbol{k_1}$	diag(245, 245, 245, 245)
$\boldsymbol{k_2}$	diag(298, 298, 298, 298)
γ_1	0.8
γ_2	1.2
Λ	60
$\boldsymbol{k_3}$	diag(3631, 3631, 3631, 3631)
N_1	1.05
N_2	0.95
σ_i	0.001
$\boldsymbol{K}_{a1}$	diag(2, 2)
$\boldsymbol{K}_{a2}$	diag(2, 2)
$\boldsymbol{K}_{u1}$	diag(2, 2)
$\boldsymbol{K}_{u2}$	diag(2, 2)
$\boldsymbol{\xi}$	diag(0.002, 0.002)
$\boldsymbol{\Gamma_1}$	diag(4, 4)
$\boldsymbol{\Gamma_2}$	diag(2, 2)
$\boldsymbol{\Gamma_3}$	diag(0.2, 0.2)
Γ_4	0.4
M_1	1.1
M_2	0.9

The trolley moves along the x-axis following an S-shaped trajectory. Meanwhile, the hoisting/lowering cable had a pimf. The initial position was $[x_0, l_0] = [0,5]$ m, and the final position was $[x_f, l_f] = [5,5]$ m. Both the initial and final velocities and accelerations were zero. The motion time along the x-axis was $t_c = 25$ s.

$$\begin{cases} x_r = x_0 + \frac{x_f}{1+e^{-0,5(t-tc)}} \\ l_{1r} = 5 + 5\mathrm{pimf}(t, [0\ 10\ 20\ 30\ 40]) \end{cases}$$

A. Results from Scenario 1

The scenario was carried out with altered system parameters, and the initial swing angle when the trolley started moving was 3°. The results obtained in Scenario 1 are shown in Figures 2 and 3.

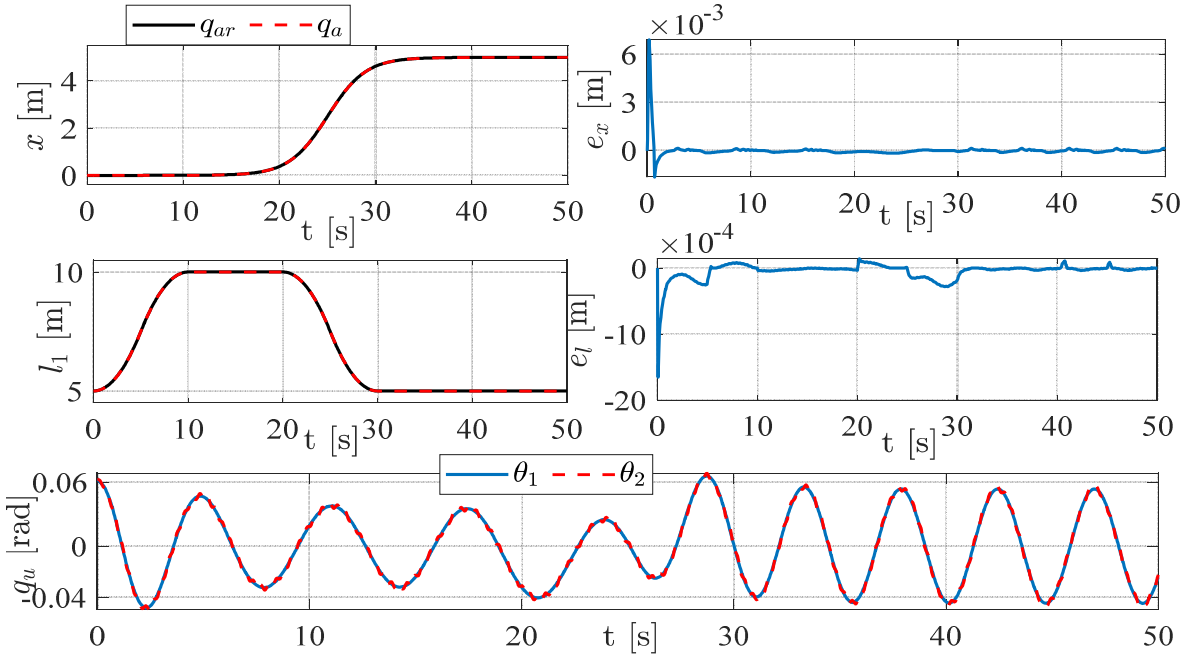

(a) Tracking trajectory and swing angle.

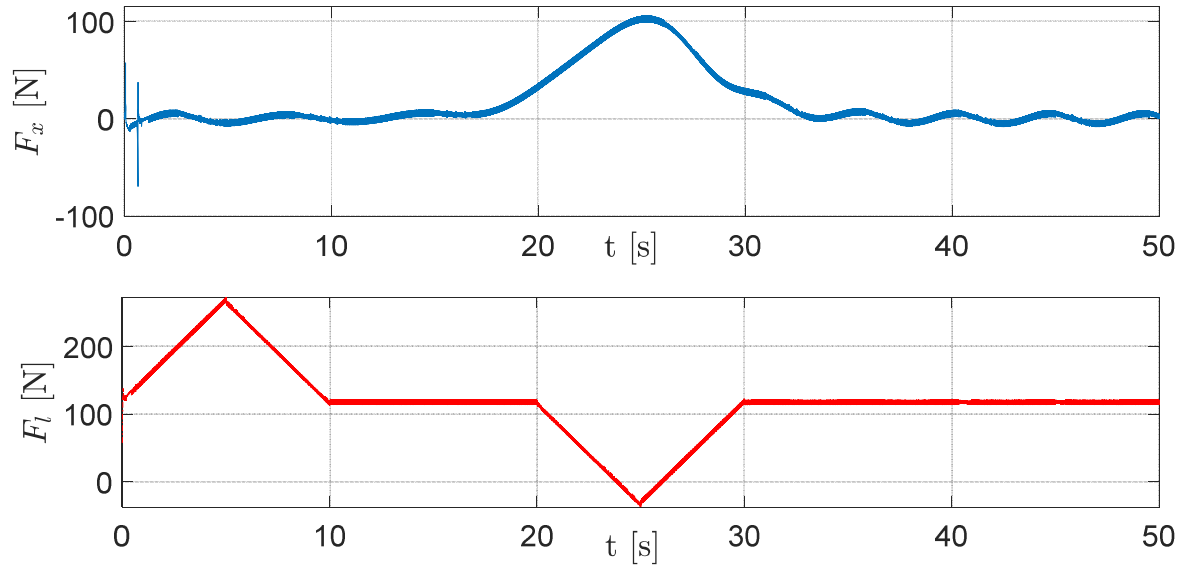

(b) Applied force.

Fig. 2. Control performance (Scenario 1).

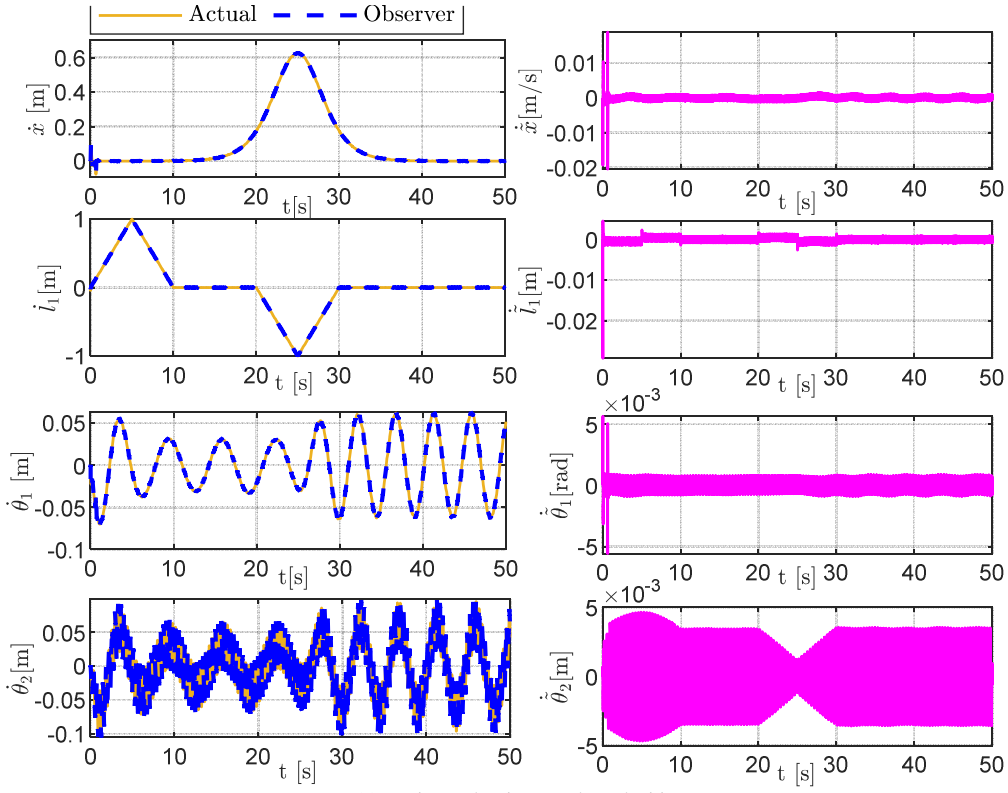

(a) Motion and swing angular velocities.

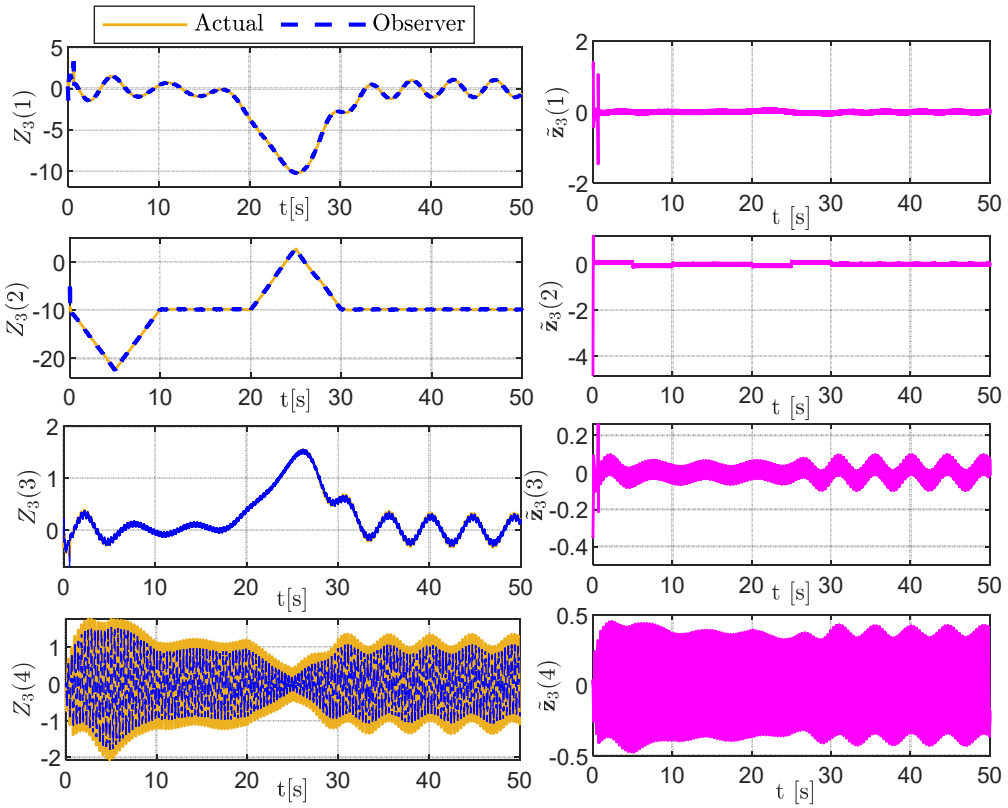

(b) Lumped disturbance.

Fig. 3. Observer performance (Scenario 1).

B. Results of Scenario 2

The system was subjected to external disturbances, as illustrated in Figure 4(a). The results obtained in Scenario 2 are depicted in Figures 4 and 5.

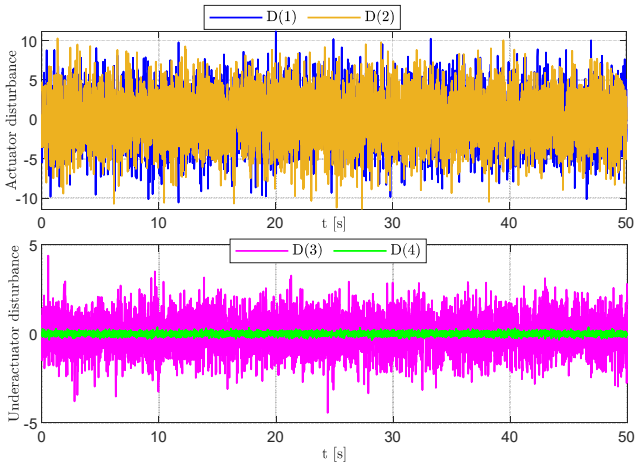

(a) White noise.

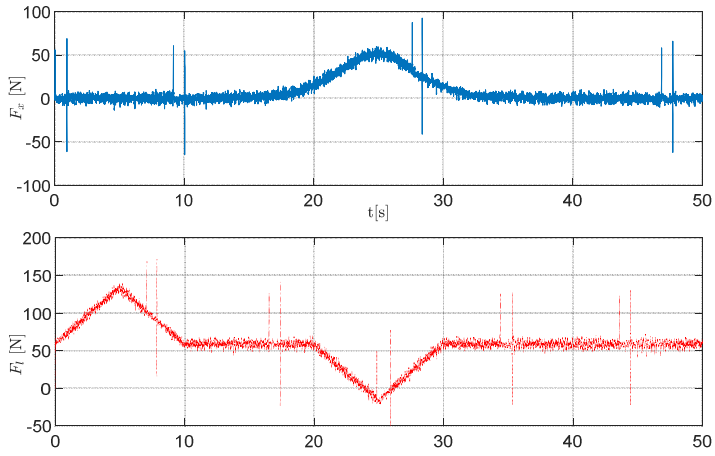

(b) Applied force.

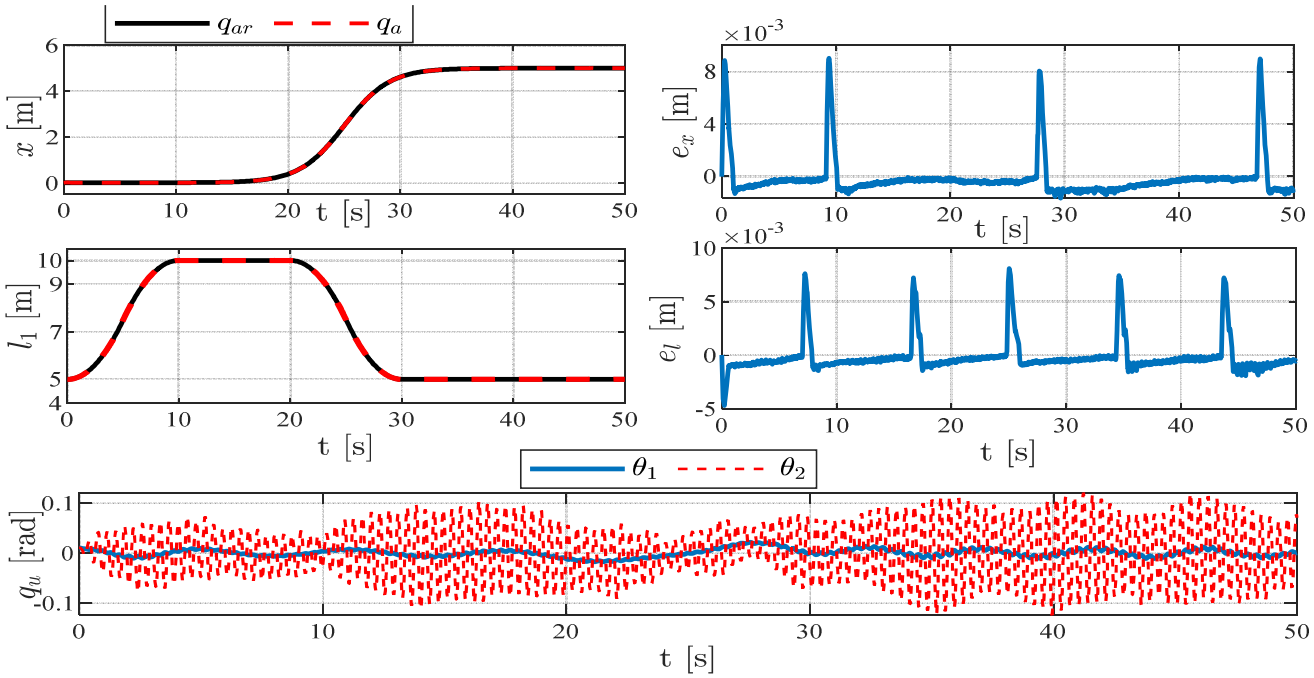

(c) Tracking trajectory and swing angle.

Fig. 4. Control performance (Scenario 2).

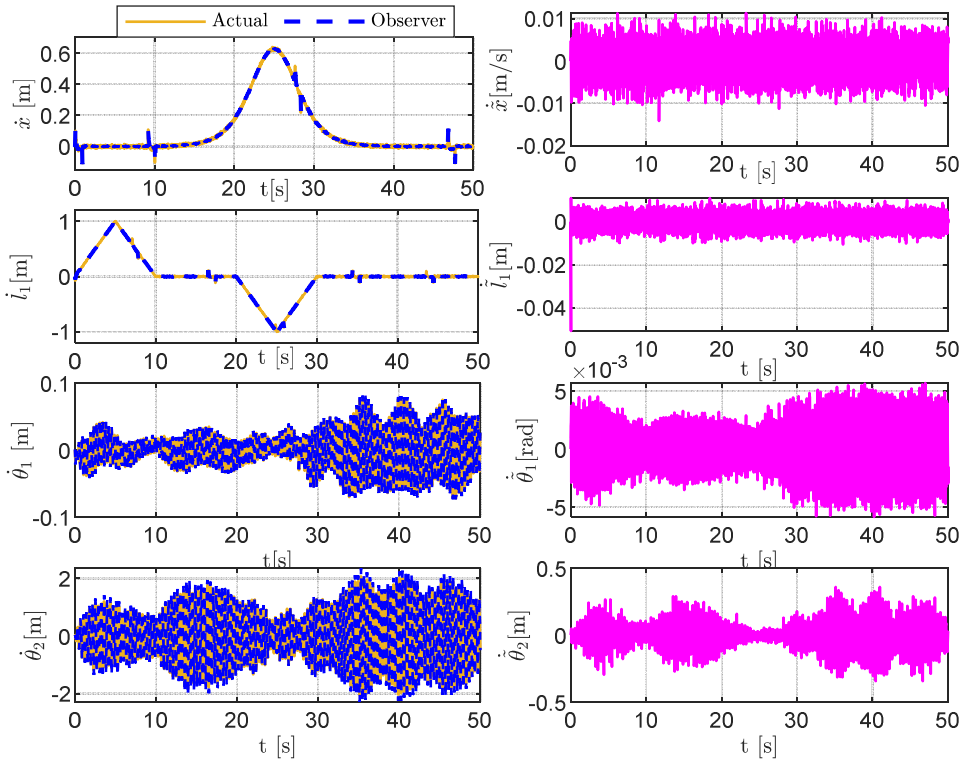

(a) Motion and swing angular velocities.

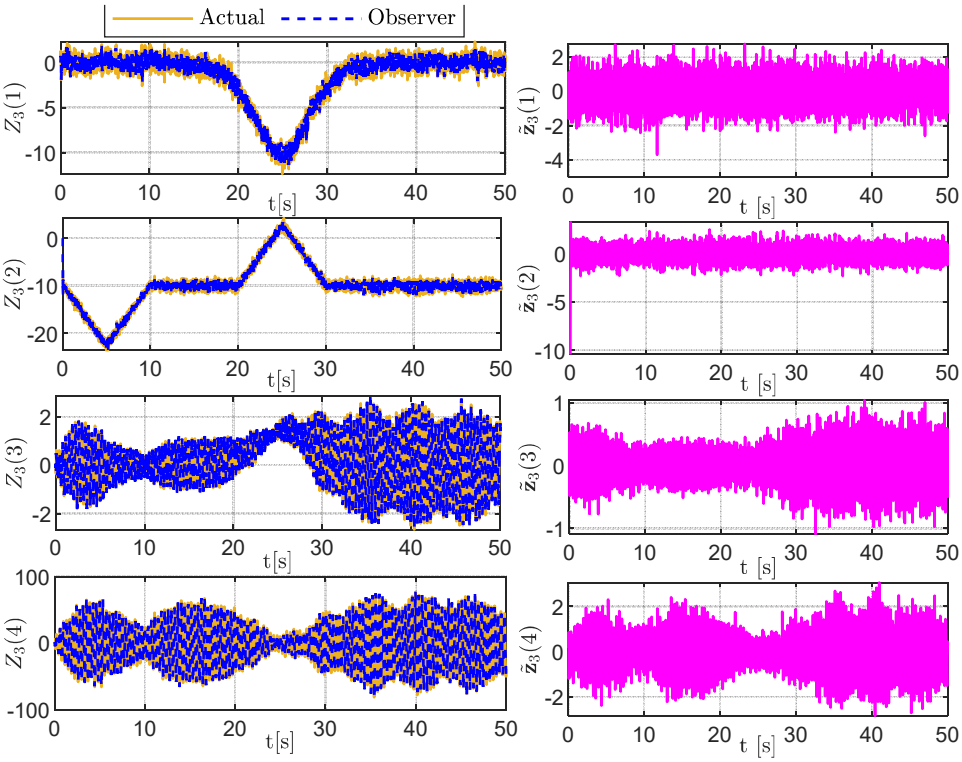

(b) Lumped disturbance.

Fig. 5. Observer performance (Scenario 2).

Based on the simulation results from both scenarios, the controller demonstrates its ability to track the trajectory shown in Figures 2(a) and 4(c). Under conditions of model uncertainty or external disturbances, the trajectory of the trolley's position

along the x-axis and the cable length l_1 consistently follow the reference trajectories to the desired positions, with control errors being very small, almost negligible. Additionally, the swing angle results for the hook and payload in Figures 29(a)-4(c) also demonstrate that, under different operating conditions, the controller consistently ensures the ability to limit and reduce the amplitude of the swing angles within an acceptable range ($< 6^0$). The control forces shown in Figures 2(b) and 4(b) illustrate the performance of the controller. The force F_x is generated appropriately, corresponding to the acceleration and deceleration of the trolley, while the force F_l reflects the necessary and reasonable adjustments for the payload hoisting/lowering trajectory. The values of these forces are all within an acceptable range, without causing large force spikes. This exhibits that the controller operates effectively and is energy-efficient.

The FxT-ESO operates with high accuracy and reliability. This is demonstrated by estimating the state variables and extended states under various operating conditions, including model uncertainty and external disturbances. As shown in Figures 3 and 5, the observation errors are very small, and the oscillations remain within an acceptable range. This confirms that the FxT-ESO is an effective tool for estimating the necessary states for controller design, reducing the number of sensors needed, and mitigating the effects of external disturbances. Thus, the simulation results indicate that the proposed controller and observer for the double-pendulum overhead crane system in two-dimensional space operate effectively under various operating conditions. The system achieves accurate trajectory tracking while suppressing the oscillations of both the hook and the payload, thanks to the reliable state estimation capability of the observer.

VI. CONCLUSIONS

This study successfully presents and validates an Adaptive Hierarchical Sliding Mode Controller (AHSMC) integrated with an Fixed-Time Extended State Observer (FxT-ESO) for a two-Dimensional Double-pendulum Overhead Crane (2DDOC) system. The performed simulations confirmed the effectiveness of the proposed approach in trajectory tracking and significant swing suppression under model uncertainties, with the FxT-ESO accurately estimating the states and disturbances. The main contribution of the current work is the novel synergistic AHSMC-FxT-ESO architecture for this application, offering two main advancements over previous work: The design ensures closed-loop system convergence within a predetermined time T_{fc}, independent of initial conditions. This is a critical theoretical advantage over both asymptotic and finite-time control, providing time-deterministic performance. The FxT-ESO enables fixed-time estimation of unmeasured states and lumped disturbances, thereby enhancing structural robustness against uncertainties and relaxes sensor requirements, which improves upon traditional state-feedback strategies. This successful validation lays a strong foundation for future hardware implementation.

ACKNOWLEDGEMENT

The author would like to sincerely thank Electric Power University for funding this research.

REFERENCES

[1] M. D. Duong, Q. T. Dao, and T. H. Do, "Settling Time Optimization of a Critically Damped System with Input Shaping for Vibration Suppression Control," *Engineering, Technology & Applied Science Research*, vol. 12, no. 5, pp. 9388–9394, Oct. 2022, https://doi.org/10.48084/etasr.5242.

[2] H. B. T. Khanh, M. H. Thi, L. T. Hue, T. L. Nguyen, and D. H. Nguyen, "Flatness-based Motion Planning and Model Predictive Control of Industrial Cranes," *Engineering, Technology & Applied Science Research*, vol. 14, no. 4, pp. 15141–15148, Aug. 2024, https://doi.org/10.48084/etasr.7662.

[3] H. Ouyang, X. Xu, and G. Zhang, "Energy-shaping-based nonlinear controller design for rotary cranes with double-pendulum effect considering actuator saturation," *Automation in Construction*, vol. 111, Mar. 2020, Art. no. 103054, https://doi.org/10.1016/j.autcon.2019.103054.

[4] M. Giacomelli, F. Padula, L. Simoni, and A. Visioli, "Simplified input-output inversion control of a double pendulum overhead crane for residual oscillations reduction," *Mechatronics*, vol. 56, pp. 37–47, Dec. 2018, https://doi.org/10.1016/j.mechatronics.2018.10.002.

[5] H. I. Jaafar, Z. Mohamed, M. A. Shamsudin, N. A. Mohd Subha, L. Ramli, and A. M. Abdullahi, "Model reference command shaping for vibration control of multimode flexible systems with application to a double-pendulum overhead crane," *Mechanical Systems and Signal Processing*, vol. 115, pp. 677–695, Jan. 2019, https://doi.org/10.1016/j.ymssp.2018.06.005.

[6] H. I. Jaafar, Z. Mohamed, M. A. Ahmad, N. A. Wahab, L. Ramli, and M. H. Shaheed, "Control of an underactuated double-pendulum overhead crane using improved model reference command shaping: Design, simulation and experiment," *Mechanical Systems and Signal Processing*, vol. 151, Apr. 2021, Art. no. 107358, https://doi.org/10.1016/j.ymssp.2020.107358.

[7] Y. Zhao, X. Wu, F. Li, and Y. Zhang, "Positioning and Swing Elimination Control of the Overhead Crane System with Double-Pendulum Dynamics," *Journal of Vibration Engineering & Technologies*, vol. 12, pp. 971–978, Jan. 2024, https://doi.org/10.1007/s42417-023-00887-8.

[8] M. Idrees, "Control of a Double-Pendulum Overhead Crane System Based on Hierarchical Sliding Mode Control Techniques," *Biophysical Reviews and Letters*, vol. 19, no. 4, pp. 375–390, Dec. 2024, https://doi.org/10.1142/S1793048023410023.

[9] Q. Wu, X. Wang, L. Hua, and M. Xia, "Modeling and nonlinear sliding mode controls of double pendulum cranes considering distributed mass beams, varying roped length and external disturbances," *Mechanical Systems and Signal Processing*, vol. 158, Sept. 2021, Art. no. 107756, https://doi.org/10.1016/j.ymssp.2021.107756.

[10] T. Wang, J. Qiu, W. Luo, and J. Zhang, "Based on the two-dimensional air resistance bridge crane anti-swing control research," *Procedia Computer Science*, vol. 183, pp. 175–181, Jan. 2021, https://doi.org/10.1016/j.procs.2021.02.047.

[11] B. Lu, Y. Fang, and N. Sun, "Enhanced-coupling adaptive control for double-pendulum overhead cranes with payload hoisting and lowering," *Automatica*, vol. 101, pp. 241–251, Mar. 2019, https://doi.org/10.1016/j.automatica.2018.12.009.

[12] X. Yao, H. Chen, Y. Liu, and Y. Dong, "Tracking approach of double pendulum cranes with variable rope lengths using sliding mode technique," *ISA Transactions*, vol. 136, pp. 152–161, May 2023, https://doi.org/10.1016/j.isatra.2022.11.019.

[13] M. Lei, X. Wu, Y. Zhao, and F. Li, "Output feedback control for overhead cranes subject to double-pendulum swing effects and uncertain disturbances," *Transactions of the Institute of Measurement and Control*, vol. 46, no. 7, pp. 1350–1361, Apr. 2024, https://doi.org/10.1177/01423312231196945.

[14] Y. Zhao, X. Wu, Y. Zhang, and L. Ke, "Lyapunov approach for the control of overhead crane systems with double-pendulum dynamics and uncertain disturbances," *Proceedings of the Institution of Mechanical Engineers, Part I: Journal of Systems and Control Engineering*, vol. 238, no. 6, pp. 1002–1012, July 2024, https://doi.org/10.1177/09596518241228331.

[15] Y. Zhang, C. Dai, and X. Wu, "Finite-time plant-parameter-free trajectory tracking control for overhead cranes with double-pendulum dynamics and uncertain disturbances," *Transactions of the Institute of Measurement and Control*, Dec. 2024, https://doi.org/10.1177/01423312241295579.

[16] Y. Xiao, C. Zhu, W. Li, and J. Xie, "Sliding mode control for double-pendulum overhead cranes with playload swing state observation," *Journal of Central South University(Science and Technology)*, vol. 52, no. 4, pp. 1129–1137, 2021, https://doi.org/10.11817/j.issn.1672-7207.2021.04.010.

[17] M. Basin, P. Yu, and Y. Shtessel, "Finite- and fixed-time differentiators utilising HOSM techniques," *IET Control Theory & Applications*, vol. 11, no. 8, pp. 1144–1152, 2017, https://doi.org/10.1049/iet-cta.2016.1256.

[18] J. Ni, L. Liu, M. Chen, and C. Liu, "Fixed-Time Disturbance Observer Design for Brunovsky Systems," *IEEE Transactions on Circuits and Systems II: Express Briefs*, vol. 65, no. 3, pp. 341–345, Mar. 2018, https://doi.org/10.1109/TCSII.2017.2710418.

[19] B. Tian, Z. Zuo, X. Yan, and H. Wang, "A fixed-time output feedback control scheme for double integrator systems," *Automatica*, vol. 80, pp. 17–24, June 2017, https://doi.org/10.1016/j.automatica.2017.01.007.

[20] Y. Huang and Y. Jia, "Fixed-time consensus tracking control for second-order multi-agent systems with bounded input uncertainties via NFFTSM," *IET Control Theory & Applications*, vol. 11, no. 16, pp. 2900–2909, 2017, https://doi.org/10.1049/iet-cta.2017.0304.

[21] Z. Anjum, Z. Sun, and B. Chen, "Disturbance-observer-based fault-tolerant control of robotic manipulator: A fixed-time adaptive approach," *IET Control Theory & Applications*, vol. 18, no. 11, pp. 1398–1413, 2024, https://doi.org/10.1049/cth2.12672.

[22] W. Wang, J. Yi, D. Zhao, and D. Liu, "Design of a stable sliding-mode controller for a class of second-order underactuated systems," *IEE Proceedings - Control Theory and Applications*, vol. 151, no. 6, pp. 683–690, Nov. 2004, https://doi.org/10.1049/ip-cta:20040902.